Local Earthquake Magnitude Scale and *b*-Value for the Danakil Region of Northern Afar

Finnigan Illsley-Kemp[1], Derek Keir[1], Jonathan M. Bull[1], Atalay Ayele[2], James O. S. Hammond[3], J-Michael Kendall[4], Ryan Gallacher[1], Thomas Gernon[1], and Berhe Goitom[4]

[1]*Ocean and Earth Science, National Oceanography Centre Southampton, University of Southampton, Southampton, UK*
[2]*Institute of Geophysics Space Science and Astronomy, Addis Ababa University, Addis Ababa, Ethiopia*
[3]*School of Earth and Planetary Sciences, Birkbeck, University of London, London, UK*
[4]*Department of Earth Sciences, University of Bristol, Bristol, UK*

Derek Keir is also at: Dipartimento di Scienze della Terra, Università degli Studi di Firenze, Florence, Italy

Abstract

The Danakil region of northern Afar is an area of ongoing seismic and volcanic activity caused by the final stages of continental breakup. To improve the quantification of seismicity we have developed a calibrated local earthquake magnitude scale. The accurate calculation of earthquake magnitudes allows the estimation of b-values and maximum magnitudes, both of which are essential for seismic hazard analysis. Earthquake data collected between February 2011 and February 2013 on 11 three-component, broadband seismometers were analyzed. A total of 4275 earthquakes were recorded over hypocentral distances ranging from 0–400 km. 32904 zero-to-peak amplitude measurements (A) were measured on the seismometer's horizontal components and were incorporated into a direct linear inversion that solved for all individual local earthquake magnitudes (M_L), 22 station correction factors (C) and 2 distance-dependent factors (n, K) in the equation: $M_L = \log(A) - \log(A_0) + C$. The resultant distance correction term is given by $-\log(A_0) = 1.274336\log(r/17) - 0.000273(r - 17) + 2$. This distance correction term suggests that attenuation in the upper and mid crust of northern Afar is relatively high, consistent with the presence of magmatic intrusions and partial melt. In contrast, attenuation in the lower crust and uppermost mantle is anomalously low, interpreted to be caused by a high melt fraction causing attenuation to occur outside the seismic frequency band. The calculated station corrections serve to reduce the M_L residuals significantly but do not show a correlation with regional geology. The cumulative seismicity rate produces a b-value of 0.9 ± 0.06 which is higher than most regions of continental rifting yet lower than values recorded at mid-ocean ridges, further supporting the hypothesis that northern Afar is transitioning to seafloor spreading.

Introduction

The Danakil region, in northern Afar is one of the few areas in the world where the transition from continental rifting to seafloor spreading is exposed subaerially. The region is seismically active and encompasses at least 24 active volcanic centres. The Ethiopian plateau, to the west of the Danakil depression, supports a significant population. Given its proximity to the western border fault of Afar, the town of Mekele faces a high level of seismic risk and experienced a swarm of earthquakes in 2002 (*Ayele et al.*, 2007). The accurate calculation of local magnitudes is a key component of seismic hazard analysis, in particular when estimating b-values and maximum magnitudes. Accurate local magnitudes are also essential for studies that attempt to understand the geological processes occurring in locations such as northern Afar, for example stress accumulation and amount of strain by faulting.

Seismic energy will attenuate at varying rates depending on factors such as temperature, composition and fluid content of the crust as well as partial melt and magmatic intrusions (*Carletti and Gasperini*, 2003; *Keir et al.*, 2006; *Schlotterbeck and Abers*, 2001; *Wang et al.*, 2009). This rate of attenuation is characterized by an attenuation curve (Fig. 3). The use of an inappropriate attenuation curve will result in errors when assigning local magnitude values to earthquakes. For two years, from 2011 to 2013, a seismic network was deployed over an area covering 260 $\times$ 150 km (Figs. 1, 2). The aim of this study is to use the seismic data recorded by eleven broadband seismometers in order to quantify seismic activity including improved estimation of local magnitudes (M_L). To do this we invert maximum body-wave amplitude and hypocentral distance information to derive a region-specific magnitude scale based on the definitions of *Richter* (1935, 1958).

Geological Setting

The Afar depression is a region that is in the late stages of continental breakup and lies at the triple junction between the Gulf of Aden, the southern Red Sea and the Main Ethiopian rift (*McKenzie and Davies*, 1970; *Mohr*, 1970). The initiation of rifting in Afar occurred between 31 and 29 Ma (*Hofmann et al.*, 1997; *Ukstins*

et al., 2002), with initial extension thought to be accommodated by large-scale border faults (*Wolfenden et al.*, 2005). In northern Afar strain localized to NNW–SSE trending, 10–30 km wide, 60–100 km long axial volcanic segments between 25 and 20 Ma (*Hayward and Ebinger*, 1996; *Wolfenden et al.*, 2005). Extension rates vary across the Danakil region with extension of ∼7 mm/yr in the northernmost area (15°N) and ∼20 mm/yr in the south (13°N), with the extension directed ENE–WSW (*McClusky et al.*, 2010). The crust thins dramatically in the Danakil depression from ∼27 km thickness in the rift to the south of the depression to <15 km beneath the depression (*Hammond et al.*, 2011; *Makris and Ginzburg*, 1987). The crust is >40 km thick beneath the Ethiopian plateau (*Corti et al.*, 2015; *Hammond et al.*, 2011).

The Danakil depression is a ∼200 km long, 50–150 km wide basin which is mostly below sea level but currently subaerial (Fig. 1). Due to the low elevation the surface sediments in the area largely consist of thick layers of evaporites formed from repeated marine incursions (*Barberi and Varet*, 1970; *Keir et al.*, 2013) most recently 32000 years ago (*Bonatti et al.*, 1971). The depression also contains the NNW–SSE trending Erta-Ale volcanic segment (EAVS) and seven active volcanoes (*Barberi and Varet*, 1970; *Nobile et al.*, 2012) (Fig. 1). The volcanic range is the focus for most of the magmatic activity in the region and is responsible for the majority of Quaternary to Recent basalts in Afar (*Bastow and Keir*, 2011). It is also thought to mark the boundary of the Danakil microplate to the east (*Eagles et al.*, 2002). Geodetic observations of Gada-Ale, Dallol and Alu-Dalafilla volcanoes in the Erta-Ale range have been successfully modelled as fluxes of magma in upper crustal reservoirs and intrusions (*Amelung et al.*, 2000; *Field et al.*, 2012; *Nobile et al.*, 2012; *Pagli et al.*, 2012).

In addition to the Erta-Ale volcanic range there are a suite of other active volcanoes in the region (Fig. 1). At the southern edge of the Danakil depression there are the Amarta-Barawli volcanic complex (ABVS), Afdera volcano (AV) and Alayta volcano (ALV) (*Barberi and Varet*, 1970). To the south of the Danakil depression in central west Afar, the rift axis steps en echelon to the southwest into the Dabbahu segment (DVS), which underwent a major dike intrusion episode

during 2005–2010 (*Barnie et al.*, 2015; *Ebinger et al.*, 2008; *Wright et al.*, 2006). Nabro volcano (NVS), which erupted in June 2011, is on the eastern margin of the Danakil depression near the Eritrean-Ethiopian border (*Goitom et al.*, 2015; *Hamlyn et al.*, 2014) (Fig. 1).

A variety of geophysical studies have shown that extension in Afar and the Main Ethiopian rift is accommodated by a combination of magmatic intrusion and lithospheric thinning (e.g., *Bastow and Keir*, 2011). There is extensive evidence, from InSAR, magnetics, receiver functions, magentotellurics and seismic anisotropy, for the presence of dikes and sills in the crust south of 13°N in Afar (*Bridges et al.*, 2012; *Desissa et al.*, 2013; *Hammond*, 2014; *Keir et al.*, 2011; *Wright et al.*, 2006). Furthermore, a study into forty years of seismicity in Afar by *Hofstetter and Beyth* (2003) found that >50% of the geodetic moment, as predicted by plate separation rates, is taken up aseismically. Along with a larger body of work these results show that magmatic processes play an important role in continental breakup (*Calais et al.*, 2008; *Thybo and Nielsen*, 2009). North of 13°N, in the Danakil depression, extensive crustal thinning is observed (*Hammond et al.*, 2011; *Makris and Ginzburg*, 1987). This suggests that ductile stretching and thinning of the crust may also play an important role in the accommodation of extension.

Many studies have attempted to investigate the thermochemical state of the mantle beneath Afar. Seismic tomography by *Bastow et al.* (2008) finds a broad low seismic velocity structure beneath the Main Ethiopian rift that extends to depths of >400 km. Tomographic studies in northern Afar also show a region of low seismic velocity from 50 km to 400 km depth, which is interpreted as a region of elevated temperature and partial melt (*Civiero et al.*, 2015; *Hammond et al.*, 2013; *Stork et al.*, 2013). This interpretation is further corroborated by modelling geochemical data that suggests an elevated mantle temperature of 1450°C (*Armitage et al.*, 2015; *Ferguson et al.*, 2013). The elevated mantle temperature will promote partial melting even at relatively low rates of extension.

Data

The seismic network comprised sixteen broadband seismometers that were operational for two years between February 2011 and February 2013 (Fig. 1). Thirteen Güralp CMG-3ESPCD instruments and three Güralp CMG-6TD instruments recorded continuous data at 50 Hz. A total of 4275 earthquakes were recorded across the network during the experiment and were located with *Hypo2000* (*Klein*, 2002). We used a 1D velocity model based on a seismic refraction survey from the area (*Makris and Ginzburg*, 1987). Accounting for instrument faults, a total of eleven seismometers were used to calculate the local magnitude scale. The velocity seismograms were convolved with the standard Wood-Anderson response, with a Wood-Anderson gain of 2800, in order to produce Wood-Anderson displacement seismograms (*Anderson and Wood*, 1925; *Kanamori and Jennings*, 1978). The maximum peak-to-peak amplitude on both the east-west and the north-south components of each station was measured, in millimeters, for each event. The final dataset consisted of 32904 amplitude measurements with hypocentral distances ranging from 0 to 420 km (Fig. 4).

Method

The definition of local magnitude, M_L, is given by *Richter* (1935, 1958):

$$M_L = \log(A) - \log(A_0) + C, \tag{1}$$

where A is the maximum zero-to-peak amplitude on the horizontal seismogram, $\log(A_0)$ is a distance correction term that is calculated empirically and C is a correction term for each component of each station, that is also calculated empirically.

Richter originally defined the local magnitude scale such that an earthquake of M_L 3 would cause a 1 mm deflection on a standard horizontal Wood-Anderson seismograph at a distance of 100 km from the hypocenter. *Hutton and Boore* (1987) observed that Richter's scale tended to underestimate magnitudes at stations close to the hypocenter and overestimate for more distant stations. To counter this

problem they developed a method to calculate how attenuation rates vary over increasing hypocentral distances, which yields an attenuation curve for specific regions. This allows for the magnitude scale to be normalized at a closer distance, thus minimizing geographical variations in wave propagation. They now define a M_L 3 earthquake as causing a 10 mm deflection on a Wood-Anderson seismograph at a distance of 17 km from the hypocenter. The distance correction term is defined as:

$$-\log(A_0) = n\log(r/17) + K(r-17) + 2, \tag{2}$$

where n and K are constants to be calculated and relate to geometrical spreading and attenuation of seismic waves, respectively, and r is the hypocentral distance in kilometers.

Combining equations 1 and 2, the observed amplitude, A_{ijk}, for each component of each station for each event can be written as:

$$\log(A_{ijk}) + 2 = -n\log(r_{ij}/17) - K(r_{ij}-17) + M_{L(i)} - C_{jk}, \tag{3}$$

where indexes i, j and k represent events, stations and components respectively. It is now possible to invert for the unknowns n, K, M_L and C. Each station has two correction terms associated with the north-south and east-west horizontal components. The set of equations includes a constraint that all station corrections sum to zero. The set of equations 3 can be combined into a matrix form, shown in Equation 4, which represents an equation $\mathbf{d} = \mathbf{m}.\mathbf{A}$ and is a system of $N_e + 2N_s + 2$ unknowns, where N_e and N_s are the number of events and stations respectively. The data from Danakil includes 4275 events recorded on 11 stations, producing a matrix with dimensions of 32904×4299 with 4299 unknowns to be solved. We then solve Equation 4 with a least-squares criterion and produce an optimal solution (*Keir et al.*, 2006).

$$\begin{pmatrix} \log(A_{111})+2 \\ \log(A_{112})+2 \\ \vdots \\ \log(A_{1N_s2})+2 \\ \log(A_{211})+2 \\ \vdots \\ \log(A_{N_eN_s2})+2 \end{pmatrix} = \begin{pmatrix} n \\ K \\ M_{L(1)} \\ M_{L(2)} \\ \vdots \\ M_{L(N_e)} \\ C_{11} \\ C_{12} \\ \vdots \\ C_{N_s2} \end{pmatrix} . \begin{pmatrix} \log(r_{11}/17) & (r_{11}-17) & 1 & 0 & \cdots & 0 & 1 & 0 & \cdots & 0 \\ \log(r_{11}/17) & (r_{11}-17) & 1 & 0 & \cdots & 0 & 0 & 1 & \cdots & 0 \\ \vdots & \vdots & \vdots & \vdots & \ddots & \vdots & \vdots & \vdots & \ddots & \vdots \\ \log(r_{1N_s}/17) & (r_{1N_s}-17) & 1 & 0 & \cdots & 0 & 0 & 0 & \cdots & 1 \\ \log(r_{21}/17) & (r_{21}-17) & 0 & 1 & \cdots & 0 & 0 & 0 & \cdots & 1 \\ \vdots & \vdots & \vdots & \vdots & \ddots & \vdots & \vdots & \vdots & \ddots & \vdots \\ \log(r_{N_eN_s}/17) & (r_{N_eN_s}-17) & 0 & 0 & \cdots & 1 & 0 & 0 & \cdots & 1 \end{pmatrix}, \tag{4}$$

Our approach differs to many previous studies which have used an iterative technique (*Baumbach et al.*, 2003; *Langston et al.*, 1998). The direct inversion method is computationally much faster and has been tested by *Pujol* (2003) on data from Tanzania that was previously analyzed using the iterative technique (*Langston et al.*, 1998). The method used in this study has been tested on data from the Main Ethiopian rift and yielded identical results to those produced by *Keir et al.* (2006).

Results

The inversion produced an equation for the distance correction term, $\log(A_0)$, for the Danakil region using a 17 km normalization:

$$-\log(A_0) = 1.274336\log(r/17) - 0.0002731(r-17) + 2. \tag{5}$$

Attenuation rates for the Danakil region (Fig. 3) are very similar to that of the Main Ethiopian rift for hypocentral distances up to ∼70 km. For larger distances the attenuation is significantly lower than in the Main Ethiopian rift (*Keir et al.*, 2006). The curve also shows that the attenuation rate in the Danakil region is significantly higher than in Tanzania (*Langston et al.*, 1998).

The effect that the newly derived attenuation curve has on magnitude estimates is shown in Figure 5. We show the magnitude residuals with increasing hypocentral distance when using the magnitude scale for the Danakil region, the Main Ethiopian

rift (*Keir et al.*, 2006) and Tanzania (*Langston et al.*, 1998). Magnitude residuals calculated with the new Danakil magnitude scale display no bias with hypocentral distance, and hence an average residual of near zero at all hypocentral distances. In contrast the Main Ethiopian rift scale overestimates magnitudes with increasing hypocentral distance and the Tanzanian scale underestimates magnitudes, as shown by the respective gradients of the residual averages in Figure 5. The average variance of the residuals for the Danakil magnitude scale is 0.2 M_L, therefore the average error in magnitude calculation is given as ± 0.2 M_L. Individual magnitude errors for each event are listed in the supplementary material. To test whether the error in magnitude is dependent on magnitude value we plot box plots of error values for events grouped at 0.5 magnitude intervals (Figure 6). This clearly shows that magnitude error is stable for the full range of magnitudes in this study. As a further test of the magnitude scale we compare GCMT moment magnitudes (M_w) from the Danakil region with local magnitude values calculated with the derived magnitude scale, Table 1. The listed events are assumed to be representative and worldwide comparisons of M_w and M_L find the two scales to be, on average, consistent for shallow earthquakes (< 33 km) (*Kanamori*, 1983).

Station Corrections

The set of equations 4, includes a station correction term C_{jk} for each component of each station. There is also a condition included that all station corrections sum to zero. The station corrections calculated for the east-west components range from 0.48 and -0.25 M_L units and the north-south component corrections range from 0.42 and -0.39 M_L units (Fig. 7). Most stations have very similar station correction values for the north-south and east-west components. Through examining the distribution of station corrections there is no obvious link between regional geology and station correction. It is therefore most likely that station correction values are dependent on very local effects, such as near surface geology and the level of coupling between the seismometer and the soil.

Magnitude residuals, the magnitude calculated at a single station minus the

average magnitude, were calculated at all stations for both the north-south and east-west components with and without station corrections (Fig. 8). Magnitude residuals calculated without station corrections have an average of almost zero (-1.3×10^{-2} M_L), and a variance of 0.096. Magnitude residuals calculated with station corrections included have an average of very nearly zero (-3.3×10^{-8} M_L) and a variance of 0.042. This shows that including the calculated station corrections brings the average residual closer to zero and reduces the variance by >64%.

Discussion

We compare the attenuation curve derived for the Danakil region to those from other regions worldwide (Fig. 3). Attenuation is significantly higher in the Danakil region than Tanzania for all hypocentral distances greater than 50 km (*Langston et al.*, 1998). The two regions are geologically very different, Tanzania is a region of early stage, non-volcanic, continental rifting of Archaean cratonic lithosphere. Archaean cratons generally consist of thick, crystalline rock with very low geothermal gradients, both of which promote low seismic attenuation. The observed difference in seismic attenuation can therefore be explained by the presence of the Tanzanian craton.

Our new attenuation curve shows that at hypocentral distances of less than 100 km the attenuation in Danakil is very similar to that in the Main Ethiopian rift and in southern California (*Hutton and Boore*, 1987; *Keir et al.*, 2006). High attenuation in southern California is explained by high geothermal gradients beneath the San Gabriel mountains (*Schlotterbeck and Abers*, 2001). In the Main Ethiopian rift, the high rate of attenuation is ascribed to the presence of magmatic intrusions and partial melt within the crust (*Keir et al.*, 2006). The Danakil region has an abundance of active volcanism and a thinned crust which suggests the presence of partial melt and high geothermal gradients. These conditions can explain the high level of attenuation at hypocentral distances less than 100 km.

The attenuation rate in Danakil is significantly lower than the Main Ethiopian rift at hypocentral distances of over 100 km. Ray paths for earthquakes with

hypocentral distances of over 100 and 150 km are shown in Figure 9. The rays at these hypocentral distances predominantly traverse from the Danakil depression in the north to the Dabbahu segment in the south. We then calculated two-dimensional travel-time curves using *MacRay* (*Luetgert*, 1992) and a velocity model based on the seismic refraction survey by *Makris and Ginzburg* (1987), the results of which are shown in Figure 10. Earthquakes at these large hypocentral distances are sampling the lower crust and uppermost mantle at a maximum depth of ∼45 km, therefore the low attenuation observed for the Danakil region is originating from these depths. A low attenuation rate could be consistent with a paucity of partial melt. However, previous geophysical work including high conductivity in magnetollurics data and high V_P/V_S of >2 imaged by receiver functions, strongly suggest that there is a large amount of melt present in the lower crust and uppermost mantle (*Desissa et al.*, 2013; *Hammond et al.*, 2011).

It is therefore unlikely that low attenuation is caused by low melt fractions. Seismic attenuation in the upper mantle is thought to occur through two potential mechanisms, grain boundary sliding (*Faul et al.*, 2004) and melt squirt (*Mavko and Nur*, 1975; *O'Connell and Budiansky*, 1977). Grain boundary sliding has been shown to cause a broad absorption peak in the seismic frequency band and so cannot explain the low attenuation that we observe (*Faul et al.*, 2004). *Hammond and Humphreys* (2000) modelled the effect that melt squirt has on attenuation in the upper mantle with melt percentages ranging from 0–3%. They demonstrate that as melt percentage increases, melt pockets become more interconnected and melt squirt can occur at a faster rate. This has the effect of pushing the frequency at which attenuation occurs towards higher frequencies and away from the seismic frequency band. This interpretation of melt squirt causing low attenuation in the seismic frequency band has also been observed at the East Pacific Rise (*Yang et al.*, 2007). We suggest that the low attenuation observed in the uppermost mantle of Danakil can therefore be explained by a high melt fraction undergoing melt squirt.

We used the new magnitude scale for the Danakil region to investigate the seismicity that occurred in the region between Feb. 2011 and Feb. 2013. Figure 11 shows the Gutenberg-Richter distribution of log of the cumulative number of

earthquakes of magnitude M_L or greater (*Gutenberg and Richter*, 1956). The time period of the study featured the eruption and associated seismic swarm of Nabro volcano (*Goitom et al.*, 2015; *Hamlyn et al.*, 2014). Eruptions at caldera systems, such as Nabro, are extremely rare and this was the first recorded eruption of Nabro volcano. Due to the infrequent nature of the eruption, inclusion of the associated seismicity would bias the Gutenberg-Richter distribution. The events associated with the Nabro eruption have therefore been removed based on their location at the volcano (Latitude: 13.1–13.6. Longitude: 41.5–41.9) (Fig. 2). We estimate the magnitude of completeness by initially using the maximum curvature method (*Wiemer and Wyss*, 2000), which corresponds to the magnitude bin with the highest event frequency. In our data this is 1.8 M_L (Fig. 11). However, *Woessner and Wiemer* (2005) report that the maximum curvature method tends to underestimate the magnitude of completeness by 0.1–0.2 magnitude units, and we therefore estimate a magnitude of completeness of 2.0 M_L. A *b*-value of 0.9 was calculated using the maximum likelihood calculation (*Aki*, 1965). We calculated an error of ± 0.06 M_L by performing a bootstrap analysis following the method of *Pickering et al.* (1995). It is important to note that *b*-values have been observed to change significantly over small distances and through time, particularly in areas of volcanic activity (*Barton et al.*, 1999; *Wyss and McNutt*, 1998; *Wyss et al.*, 2001).

The Danakil region has a higher *b*-value than most other areas in the East African rift. South Sudan, Tanzania and Kenya, which are all regions of continental rifting, have *b*-values that range from 0.7–0.9 (*Ayele and Kulhanek*, 1997; *Langston et al.*, 1998; *Tongue et al.*, 1992). It is also significantly higher than other continental rift systems such as the Rio Grande and Eger rifts, both of which exhibit *b*-values of 0.8 (*Ibs-von Seht et al.*, 2008). In these regions rifting is less developed and also less magmatically accommodated. A lack of magmatic activity during rifting allows greater stresses to accumulate in the crust, facilitating larger earthquakes and a lower *b*-value.

The *b*-value for Danakil is lower than values recorded at mid-ocean ridges. At the Mid-Atlantic ridge, *b*-values have been observed to vary but they are consistently above 1 and can reach values of up to 1.5 (*Barclay et al.*, 2001; *Kong et al.*, 1992;

Tilmann et al., 2004). *Wilcock et al.* (2002) performed a microearthquake study on the Endeavour segment of the Juan de Fuca Ridge and recorded a b-value of 1.06. These b-values suggest that seismic energy at ocean ridges is primarily released through swarms of relatively low-magnitude earthquakes. The observation that the b-value for the Danakil region lies between those found at mid-ocean ridges and at regions of continental rifting, suggests that the Danakil region is at the transition from continental rifting to seafloor spreading.

The calculation of accurate local earthquake magnitudes is essential for estimating maximum magnitudes and for better quantification of time-space variations in seismicity b-values. As population grows in Afar and the Ethiopian plateau, more accurate quantification of earthquakes will aid seismic hazard assessment in the region (e.g., *Ayele et al.*, 2007, 2015; *Hagos et al.*, 2006).

Conclusions

We have calculated the first local magnitude scale for the Danakil region of northern Afar. The study used 32904 amplitude measurements, from 4275 earthquakes on 11 seismometers and yields the equation:

$$-\log(A_0) = 1.274336\log(r/17) - 0.000273(r-17) + 2, \tag{6}$$

where r is the hypocentral distance from station to earthquake. This equation and the corresponding attenuation curve show that the attenuation rate of seismic energy in Danakil is relatively high in the crust consistent with the presence of magmatic intrusions and melt. The relatively low attenuation observed at greater depths could indicate a low melt percentage, inconsistent with independent geophysical data. We therefore suggest that the low attenuation rate is due to a sufficiently high melt fraction in the upper mantle beneath Danakil undergoing melt squirt and causing the seismic attenuation to occur outside the seismic frequency band.

We used the seismicity in Danakil to produce a Gutenberg-Richter relationship. The catalog is complete above M_L 2.0 and the calculated b-value is given

as 0.9 ± 0.06. Our b-value is consistent with the area transitioning to sea floor spreading. Our improved magnitude scale and seismicity rate are critical for better quantification of seismic hazard. These results will also help quantify the distribution and amount of seismic strain.

Data and Resources

- Seismograms used in this study were collected as part of the Afar0911 experiment using SEIS-UK instruments. Seismic data is currently restricted but will be uploaded to IRIS in March 2016.
- Plots were made using the Generic Mapping Tools version 4.5.8 (www.soest.hawaii.edu/gmt; Wessel and Smith, 1998).

Acknowledgements

We thank SEIS-UK for use of the instruments and their computing facilities. The facilities of SEIS-UK are supported by the Natural Environment Research Council (NERC) under agreement R8/H10/64. FIK is funded through NERC studentship NE/L002531/1 and a grant to GSNOCS from Roy Franklin O.B.E. DK is supported by NERC grant NE/L013932. Funding for fieldwork is from BHP Billiton. We also acknowledge assistance from Addis Ababa University and the Afar National Regional State Government.

References

Aki, K., Maximum Likelihood Estimate of b in the Formula logN= a-bM and its Confidence Limits, *Bull. Earthquake Res. Inst. Univ. Tokyo*, *43*(237–239), 1965.

Amelung, F., C. Oppenheimer, P. Segall, and H. Zebker, Ground deformation near Gada 'Ale Volcano, Afar, observed by radar iinterferometry, *Geophys. Res. Lett.*, *27*(19), 3093–3096, 2000.

Anderson, J., and H. O. Wood, Description and theory of the torsion seismometer, *Bull. Seis. Soc. Am.*, *15*(1), 1–72, 1925.

Armitage, J. J., D. J. Ferguson, S. Goes, J. O. S. Hammond, E. Calais, C. A. Rychert, and N. Harmon, Upper mantle temperature and the onset of extension and break-up in Afar, Africa, *Earth Planet. Sci. Lett.*, *418*, 78–90, 2015.

Ayele, A., and O. Kulhanek, Spatial and temporal variation of seismicity in the Horn of Africa from 1960 to 1993, *Geophys. J. Int.*, *130*, 805–810, 1997.

Ayele, A., G. Stuart, I. Bastow, and D. Keir, The August 2002 earthquake sequence in north Afar: insights into the neotectonics of the Danakil microplate, *J. Afr. Earth Sci.*, *40*, 70–79, 2007.

Ayele, A., C. J. Ebinger, C. van Alstyne, D. Keir, C. W. Nixon, M. Belachew, and J. O. S. Hammond, Seismicity of the central Afar rift and implications for Tendaho dam hazards, *Geol. Soc. Spec. Pub.*, *420*, SP420–9, 2015.

Barberi, F., and J. Varet, The Erta Ale volcanic range (Danakil depression, northern Afar, Ethiopia), *Bulletin Volcanologique*, *34*(4), 848–917, 1970.

Barclay, A. H., D. R. Toomey, and S. C. Solomon, Microearthquake characteristics and crustal Vp/Vs structure at the Mid-Atlantic Ridge, 35 N, *J. Geophys. Res.*, *106*(B2), 2017–2034, 2001.

Barnie, T. D., D. Keir, I. Hamling, B. Hofmann, M. Belachew, S. Carn, D. Eastwell, J. O. S. Hammond, A. Ayele, C. Oppenheimer, T. Wright, A multidisciplinary study of the final episode of the Manda Hararo dyke sequence, Ethiopia, and

implications for trends in volcanism during the rifting cycle, *Geological Society, London, Special Publications*, *420*, SP420–6, 2015.

Barton, D., G. Foulger, J. Henderson, and B. Julian, Frequency–magnitude statistics and spatial correlation dimensions of earthquakes at Long Valley caldera, California, *Geophys. J. Int.*, *138*(2), 563–570, 1999.

Bastow, I., and D. Keir, The protracted development of the continent-ocean transition in Afar, *Nat. Geosci.*, *4*, 248–250, 2011.

Bastow, I., A. Nyblade, G. Stuart, T. Rooney, and M. Benoit, Upper Mantle Seismic Structure Beneath the Ethiopian Hotspot: Rifting at the Edge of the African Low Velocity Anomaly, *Geochem. Geophys. Geosyst.*, *9*(12), Q12022, doi:10.1029/2008GC002107, 2008.

Baumbach, M., D. Bindi, H. Grosser, C. Milkereit, S. Parolai, R. Wang, S. Karakisa, S. Zünbül, and J. Zschau, Calibration of an M_L scale in northwestern Turkey from 1999 Izmit aftershocks, *Bull. Seis. Soc. Am.*, *93*(5), 2289–2295, 2003.

Bonatti, E., C. Emiliani, G. Ostlund, and H. Rydell, Final desiccation of the Afar rift, Ethiopia, *Science*, *172*(3982), 468–469, 1971.

Bridges, D., K. Mickus, S. Gao, M. Abdelsalam, and A. Alemu, Magnetic stripes of a transitional continental rift in Afar, *Geology*, *40*(3), 203–206, 2012.

Calais, E., et al., Strain accommodation by slow slip and dyking in a youthful continental rift, East Africa, *Nature*, *456*, 7223, 2008.

Carletti, F., and P. Gasperini, Lateral variations of seismic intensity attenuation in Italy, *Geophys. J. Int.*, *155*(3), 839–856, 2003.

Civiero, C., J. O. S. Hammond, S. Goes, S. Fishwick, A. Ahmed, A. Ayele, C. Doubre, B. Goitom, D. Keir, J-M. Kendall, S. Leroy, G. Ogubazghi, G. Rümpker, G. W. Stuart, Multiple mantle upwellings in the transition zone beneath the northern East African Rift System from relative P wave travel time tomography, *Geochem. Geophys. Geosyst.*, 2015.

Corti, G., A. Agostini, D. Keir, J. Van Wijk, I. D. Bastow, and G. Ranalli, Magma-induced axial subsidence during final-stage rifting: Implications for the development of seaward-dipping reflectors, *Geosphere*, *11*(3), 563–571, 2015.

Desissa, M., N. Johnson, K. Whaler, S. Hautot, S. Fisseha, and G. Dawes, A mantle magma reservoir beneath an incipient mid-ocean ridge in Afar, Ethiopia, *Nat. Geosci.*, *6*(10), 861–865, 2013.

Eagles, G., R. Gloaguen, and C. Ebinger, Kinematics of the Danakil microplate, *Earth Planet. Sci. Lett.*, *203*, 607–620, 2002.

Ebinger, C. J., D. Keir, A. Ayele, E. Calais, T. J. Wright, M. Belachew, J. O. S. Hammond, E. Campbell, and W. Buck, Capturing magma intrusion and faulting processes during continental rupture: seismicity of the Dabbahu (Afar) rift, *Geophys. J. Int.*, *174*(3), 1138–1152, doi:10.1111/j.1365-246X.2008.03877.x, 2008.

Faul, U. H., F. Gerald, D. John, and I. Jackson, Shear wave attenuation and dispersion in melt-bearing olivine polycrystals: 2. Microstructural interpretation and seismological implications, *J. Geophys. Res.*, *109*(B6), 2004.

Ferguson, D. J., J. Maclennan, I. Bastow, D. Pyle, S. Jones, D. Keir, J. Blundy, T. Plank, and G. Yirgu, Melting during late-stage rifting in Afar is hot and deep, *Nature*, *499*(7456), 70–73, 2013.

Field, L., T. Barnie, J. Blundy, R. A. Brooker, D. Keir, E. Lewi, and K. Saunders, Integrated field, satellite and petrological observations of the November 2010 eruption of Erta Ale, *Bull. Volc.*, *74*(10), 2251–2271, 2012.

Goitom, B., C. Oppenheimer, J. O. S. Hammond, R. Grandin, T. Barnie, A. Donovan, G. Ogubazghi, E. Yohannes, G. Kibrom, J.-M. Kendall, S. Carn, D. Fee, C. Sealing, D. Keir, A. Ayele, J. Blundy, J. Hamlyn, T. Wright, S. Berhe, First recorded eruption of Nabro volcano, Eritrea, 2011, *Bull. Volc.*, *77*(10), 1–21, 2015.

Gutenberg, B., and C. F. Richter, Earthquake magnitude, intensity, energy, and acceleration, *Bull. Seis. Soc. Am.*, *46*(2), 105–145, 1956.

Hagos, L., R. Arvidsson, and R. Roberts, Application of the spatially smoothed seismicity and Monte Carlo methods to estimate the seismic hazard of Eritrea and the surrounding region, *Natural hazards*, *39*(3), 395–418, 2006.

Hamlyn, J. E., D. Keir, T. J. Wright, J. W. Neuberg, B. Goitom, J. O. S. Hammond, C. Pagli, C. Oppenheimer, J. Kendall, R. Grandin, Seismicity and subsidence following the 2011 Nabro eruption, Eritrea: Insights into the plumbing system of an off-rift volcano, *J. Geophys. Res.*, *119*(11), 8267–8282, 2014.

Hammond, J. O. S., Constraining melt geometries beneath the Afar Depression, Ethiopia from teleseismic receiver functions: The anisotropic H-κ stacking technique, *Geochem. Geophys. Geosyst.*, *15*(4), 1316–1332, 2014.

Hammond, J. O. S., J.-M. Kendall, G. Stuart, D. Keir, C. Ebinger, A. Ayele, and M. Belachew, The nature of the crust beneath the Afar triple junction: Evidence from receiver functions, *Geochem. Geophys. Geosyst.*, *12*(12), 2011.

Hammond, J. O. S., J.-M. Kendall, G. Stuart, C. Ebinger, I. Bastow, D. Keir, A. Ayele, M. Belachew, B. Goitom, G. Ogubazghi, T. Wright, Mantle upwelling and initiation of rift segmentation beneath the Afar Depression, *Geology*, *41*(6), 635–638, 2013.

Hammond, W. C., and E. D. Humphreys, Upper mantle seismic wave attenuation-Effects of realistic partial melt distribution, *J. Geophys. Res.*, *105*(10), 987–10, 2000.

Hayward, N., and C. Ebinger, Variations in the along–axis segmentation of the Afar rift system, *Tectonics*, *15*, 244–257, 1996.

Hofmann, C., V. Courtillot, G. Feraud, P. Rochette, G. Yirgu, E. Ketefo, and R. Pik, Timing of the Ethiopian flood basalt event and implications for plume birth and global change, *Nature*, *389*, 838–841, 1997.

Hofstetter, R., and M. Beyth, The Afar Depression: interpretation of the 1960-2000 earthquakes, *Geophys. J. Int.*, *155*(2), 715–732, 2003.

Hutton, L., and D. M. Boore, The M_L scale in southern California, *Bull. Seis. Soc. Am.*, *77*(6), 2074–2094, 1987.

Ibs-von Seht, M., T. Plenefisch, and K. Klinge, Earthquake swarms in continental rifts - a comparison of selected cases in America, Africa and Europe, *Tectonophysics*, *452*(1), 66–77, 2008.

Kanamori, H., Magnitude scale and quantification of earthquakes, *Tectonophysics*, *93*(3), 185–199, 1983.

Kanamori, H., and P. C. Jennings, Determination of local magnitude, M_L, from strong-motion accelerograms, *Bull. Seis. Soc. Am.*, *68*(2), 471–485, 1978.

Keir, D., G. Stuart, A. Jackson, and A. Ayele, Local Earthquake Magnitude Scale and Seismicity Rate for the Ethiopian Rift, *Bull. Seis. Soc. Am.*, *96*(6), 2221–2230, 2006.

Keir, D., M. Belachew, C. Ebinger, J.-M. Kendall, J. O. S. Hammond, G. W. Stuart, A. Ayele, and J. Rowland, Mapping the evolving strain field during continental breakup from crustal anisotropy in the Afar Depression, *Nature Communications*, *2*, 285, 2011.

Keir, D., I. D. Bastow, C. Pagli, and E. L. Chambers, The development of extension and magmatism in the Red Sea rift of Afar, *Tectonophysics*, *607*, 98–114, 2013.

Klein, F., *User's guide to HYPOINVERSE-2000: A Fortran program to solve for earthquake locations and magnitudes*, 1-123 pp., US Geological Survey Open File Rept. 02-171, 2002.

Kong, L. S., S. C. Solomon, and G. Purdy, Microearthquake characteristics of a mid-ocean ridge along-axis high, *J. Geophys. Res.*, *97*(B2), 1659–1685, 1992.

Langston, C. A., R. Brazier, A. A. Nyblade, and T. J. Owens, Local magnitude scale and seismicity rate for Tanzania, East Africa, *Bull. Seis. Soc. Am.*, *88*(3), 712–721, 1998.

494 Luetgert, J. H., MacRay; interactive two-dimensional seismic raytracing for the
495 Macintosh, *Tech. rep.*, US Geological Survey; Books and Open-File Reports Sec-
496 tion, 1992.

497 Makris, J., and A. Ginzburg, The Afar Depression: transition between continental
498 rifting and sea floor spreading, *Tectonophysics*, *141*, 199–214, 1987.

499 Mavko, G., and A. Nur, Melt squirt in the asthenosphere, *J. Geophys. Res.*, *80*(11),
500 1444–1448, 1975.

501 McClusky, S., R. Reilinger, G. Ogubazghi, A. Amleson, B. Healeb, P. Vernant,
502 J. Sholan, S. Fisseha, L. Asfaw, R. Bendick, L. Kogan, Kinematics of the southern
503 Red Sea–Afar Triple Junction and implications for plate dynamics, *Geophys. Res.*
504 *Lett.*, *37*(5), 2010.

505 McKenzie, D., and D. Davies, Plate tectonics of the Red Sea and east Africa,
506 *Nature*, *226*, 243–248, 1970.

507 Mohr, P., The Afar Triple Junction and sea-floor spreading, *J. Geophys. Res.*,
508 *75*(35), 7340–7352, 1970.

509 Nobile, A., C. Pagli, D. Keir, T. J. Wright, A. Ayele, J. Ruch, and V. Acocella,
510 Dike-fault interaction during the 2004 Dallol intrusion at the northern edge of
511 the Erta Ale Ridge (Afar, Ethiopia), *Geophys. Res. Lett.*, *39*(19), 2012.

512 O'Connell, R. J., and B. Budiansky, Viscoelastic properties of fluid-saturated
513 cracked solids, *J. Geophys. Res.*, *82*(36), 5719–5735, 1977.

514 Pagli, C., T. J. Wright, C. J. Ebinger, S.-H. Yun, J. R. Cann, T. Barnie, and
515 A. Ayele, Shallow axial magma chamber at the slow-spreading Erta Ale Ridge,
516 *Nat. Geosci.*, *5*(4), 284–288, 2012.

517 Pickering, G., J. Bull, and D. Sanderson, Sampling power-law distributions,
518 *Tectonophysics*, *248*(1), 1–20, 1995.

519 Pujol, J., Determination of a local magnitude scale: a generalized inverse solution,
520 *Bull. Seis. Soc. Am.*, *93*(6), 2758–2761, 2003.

Richter, C., An instrumental earthquake magnitude scale, *Bull. Seis. Soc. Am.*, *25*(1), 1–32, 1935.

Richter, C. F., *Elementary Seismology*, W. H. Freeman and Co., 1958.

Schlotterbeck, B. A., and G. A. Abers, Three-dimensional attenuation variations in southern California, *J. Geophys. Res.*, *106*(B12), 30,719–30,735, 2001.

Stork, A., G. Stuart, C. Henderson, D. Keir, and J. O. S. Hammond, Uppermost mantle (Pn) velocity model for the Afar region, Ethiopia: an insight into rifting processes, *Geophys. J. Int.*, *193*(1), 321–328, 2013.

Thybo, H., and C. Nielsen, Magma-compensated crustal thinning in continental rift zones, *Nature*, *457*, 7231, 2009.

Tilmann, F., E. Flueh, L. Planert, T. Reston, and W. Weinrebe, Microearthquake seismicity of the Mid-Atlantic Ridge at 5 S: A view of tectonic extension, *J. Geophys. Res.*, *109*(B6), 2004.

Tongue, J., P. Maguire, and P. Young, Seismicity distribution from temporary earthquake recording networks in Kenya, *Tectonophysics*, *204*(1), 71–79, 1992.

Ukstins, I., P. Renne, E. Wolfenden, J. Baker, D. Ayalew, and M. Menzies, Matching conjugate volcanic rifted margins: $^{40}Ar/^{39}Ar$ chrono stratigraphy of pre– and syn–rift bimodal flood volcanism in Ethiopia and Yemen, *Earth Planet. Sci. Lett.*, *198*, 289–306, 2002.

Wang, Y., D. Forsyth, and B. Savage, Convective upwelling in the mantle beneath the Gulf of California, *Nature*, *462*, 7272, 2009.

Wiemer, S., and M. Wyss, Minimum magnitude of completeness in earthquake catalogs: examples from Alaska, the western United States, and Japan, *Bull. Seis. Soc. Am.*, *90*(4), 859–869, 2000.

Wilcock, W. S., S. D. Archer, and G. Purdy, Microearthquakes on the Endeavour segment of the Juan de Fuca Ridge, *J. Geophys. Res.*, *107*(B12), EPM–4, 2002.

Woessner, J., and S. Wiemer, Assessing the quality of earthquake catalogues: Estimating the magnitude of completeness and its uncertainty, *Bull. Seis. Soc. Am.*, *95*(2), 684–698, 2005.

Wolfenden, E., C. Ebinger, G. Yirgu, P. Renne, and S. Kelley, Evolution of a volcanic rifted margin: Southern Red Sea, Ethiopia, *Bull. Geol. Soc. Am.*, *117*(7-8), 846–864, 2005.

Wright, T., C. Ebinger, J. Biggs, A. Ayele, G. Yirgu, D. Keir, and A. Stork, Magma-maintained rift segmentation at continental rupture in the 2005 Afar dyking episode, *Nature*, *442*(7100), 291–294, 2006.

Wyss, M., and S. R. McNutt, Temporal and three-dimensional spatial analyses of the frequency–magnitude distribution near Long Valley Caldera, California, *Geophys. J. Int.*, *134*(2), 409–421, 1998.

Wyss, M., F. Klein, K. Nagamine, and S. Wiemer, Anomalously high *b*-values in the South Flank of Kilauea volcano, Hawaii: evidence for the distribution of magma below Kilauea's East rift zone, *J. Volc. Geoth. Res.*, *106*(1), 23–37, 2001.

Yang, Y., D. W. Forsyth, and D. S. Weeraratne, Seismic attenuation near the East Pacific Rise and the origin of the low-velocity zone, *Earth Planet. Sci. Lett.*, *258*(1), 260–268, 2007.

Mailing Addresses

Finnigan Illsley-Kemp, F.Illsley-Kemp@soton.ac.uk, Ocean and Earth Science, National Oceanography Centre Southampton, University of Southampton, Southampton, UK, SO14 3ZH

Derek Keir, D.Keir@soton.ac.uk, Ocean and Earth Science, National Oceanography Centre Southampton, University of Southampton, Southampton, UK, SO14 3ZH

Jonathan M. Bull, bull@noc.soton.ac.uk, Ocean and Earth Science, National Oceanography Centre Southampton, University of Southampton, Southampton, UK, SO14 3ZH

Atalay Ayele, atalay.ayele@aau.edu.et, Institute of Geophysics Space Science and Astronomy, Addis Ababa University, Addis Ababa, Ethiopia

James O. S. Hammond, j.hammond@ucl.ac.uk, Department of Earth and Planetary Sciences, Birkbeck, University of London, Malet Street, London, WC1E 7HX.

J-Michael Kendall, gljmk@bristol.ac.uk, Department of Earth Sciences, University of Bristol, Bristol, UK, BS8 1RJ

Ryan Gallacher, R.Gallacher@soton.ac.uk, Ocean and Earth Science, National Oceanography Centre Southampton, University of Southampton, Southampton, UK, SO14 3ZH

Thomas Gernon, Thomas.Gernon@noc.soton.ac.uk, Ocean and Earth Science, National Oceanography Centre Southampton, University of Southampton, Southampton, UK, SO14 3ZH

Berhe Goitom, bg12363@bristol.ac.uk, Department of Earth Sciences, Univer-

sity of Bristol, Bristol, UK, BS8 1RJ

Table 1
A comparison between independently calculated moment magnitudes and local magnitudes

Date and Time	**Moment Magnitude** M_w[†]	**Local Magnitude** M_L[‡]	**Depth (km)**
2011/06/12 15:37:04	5.1	5.2	12
2011/06/12 19:21:50	5	5	1
2011/06/12 20:32:40	5.6	5.5	1
2011/06/12 21:03:23	5.4	5.7	2
2011/06/17 09:16:12	5.6	5.8	1

The events occurring on 2011/06/12 are associated with the eruption of Nabro volcano.
[†] Moment magnitude calculated by GCMT and USGS.
[‡] Local magnitude calculated with local magnitude scale derived from this study.

597

1. Figure 1: The seismic network deployed for this study. The network was in place between February 2011 and February 2013. Stations marked with an asterisks had one or more faulty horizontal components and so were not used for calculating magnitudes. The region contains the Erta-Ale volcanic segment (EAVS), the Dabbahu volcanic segment (DVS), Nabro volcano (NVS), the Amarta-Barawli volcanic complex (ABVS), Afdera volcano (AV) and Alayta volcano (ALV). Topography data is taken from NASA's Shuttle Radar Topography Mission (SRTM).

2. Figure 2: Locations and respective magnitudes of the 4275 earthquakes recorded in the two years between February 2011 and February 2013. All earthquakes have a minimum of four phases recorded on a minimum of three stations. The black box outlines those earthquakes associated with the eruption of Nabro volcano.

3. Figure 3: Comparison of attenuation curves for the Danakil region (this study), the Main Ethiopian rift (*Keir et al.*, 2006), Tanzania (*Langston et al.*, 1998) and southern California (*Hutton and Boore*, 1987; *Richter*, 1958). The attenuation rate in Danakil is significantly lower than the Main Ethiopian rift for hypocentral distances >70 km.

4. Figure 4: Magnitudes and hypocentral distances for the horizontal components for all stations. Magnitudes are calculated using the magnitude scale for the Danakil region.

5. Figure 5: Magnitude residuals calculated for all events using three different scales; the newly derived magnitude scale for (A) Danakil, (B) the Main Ethiopian rift magnitude scale (*Keir et al.*, 2006) and (C) the Tanzania magnitude scale (*Langston et al.*, 1998). The Danakil magnitude scale minimizes residuals at all hypocentral distances whereas the Main Ethiopian rift scale and Tanzania scale overestimate and underestimate magnitudes respectively.

6. Figure 6: Box plot of magnitude error versus magnitude, binned in 0.5 M_L intervals. Box height represents the interquartile range and whiskers represent extreme values that are within 1.5 interquartile range. Magnitude errors are

clearly shown to be stable for the reported magnitude range.

7. Figure 7: Variation of station corrections across the network. (a) North-south component corrections. (b) East-west component corrections. There is no clear correlation between regional geology and station correction. The corrections are therefore likely controlled by very local geology and site specific variables.

8. Figure 8: (a) Magnitude residuals calculated with station corrections. (b) Magnitude residuals calculated without station corrections. Magnitude residuals calculated with station corrections sum to nearly zero and the variance (0.042) has been reduced by >64% when compared to the variance without station corrections (0.096).

9. Figure 9: The ray paths for earthquakes with hypocentral distances over (a) 100 km and (b) 150 km. The ray paths predominantly traverse the Danakil depression and Dabbahu segment region.

10. Figure 10: (a) Travel-time curves for an earthquake occurring in the north of the Danakil depression. The S-waves sample the uppermost mantle at hypocentral distances >100 km, reaching depths of up to 40 km. (b) Travel-time curves for an earthquake occurring in the south of the study area. The S-waves sample the uppermost mantle at hypocentral distances >125 km, reaching depths of up to 45 km. Layer P-wave velocities are given in km s^{-1} taken from *Makris and Ginzburg* (1987).

11. Figure 11: Analysis of earthquake magnitude distribution of earthquakes in the Danakil region, excluding those associated with the eruption of Nabro on 12 June 2011. Left axes - Gutenberg-Richter distribution where log(N) represents the log of the cumulative number of earthquakes of magnitude M_L or greater. Right axes - Number of events represents the frequency of events in each magnitude bin. The magnitude of completeness (2.0 M_L) is calculated using the maximum curvature method (*Wiemer and Wyss*, 2000). We calculate the *b*-value using the maximum likelihood method. The calculated *b*-value suggests that geodetic strain is primarily released through swarms of

low magnitude earthquakes, rather than large-scale faulting.

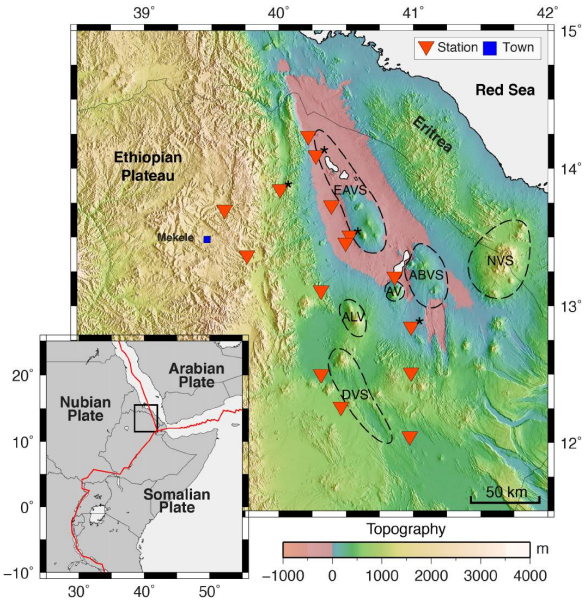

Figure 1: The seismic network deployed for this study. The network was in place between February 2011 and February 2013. Stations marked with an asterisks had one or more faulty horizontal components and so were not used for calculating magnitudes. The region contains the Erta-Ale volcanic segment (EAVS), the Dabbahu volcanic segment (DVS), Nabro volcano (NVS), the Amarta-Barawli volcanic complex (ABVS), Afdera volcano (AV) and Alayta volcano (ALV). Topography data is taken from NASA's Shuttle Radar Topography Mission (SRTM).

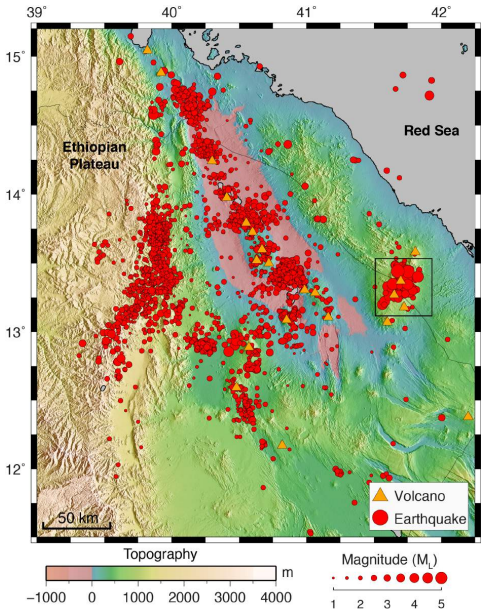

Figure 2: Locations and respective magnitudes of the 4275 earthquakes recorded in the two years between February 2011 and February 2013. All earthquakes have a minimum of four phases recorded on a minimum of three stations. The black box outlines those earthquakes associated with the eruption of Nabro volcano.

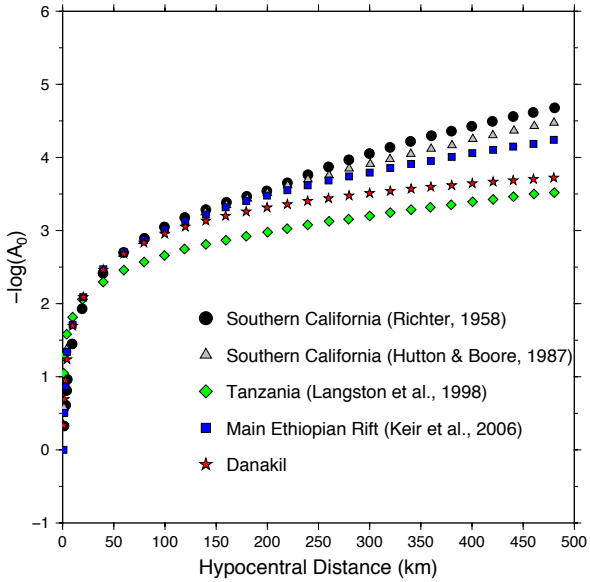

Figure 3: Comparison of attenuation curves for the Danakil region (this study), the Main Ethiopian rift (*Keir et al.*, 2006), Tanzania (*Langston et al.*, 1998) and southern California (*Hutton and Boore*, 1987; *Richter*, 1958). The attenuation rate in Danakil is significantly lower than the Main Ethiopian rift for hypocentral distances >70 km.

[p]

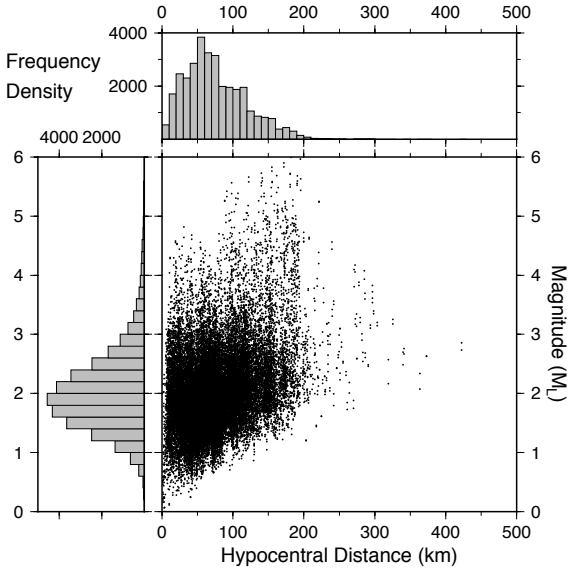

Figure 4: Magnitudes and hypocentral distances for the horizontal components for all stations. Magnitudes are calculated using the magnitude scale for the Danakil region.

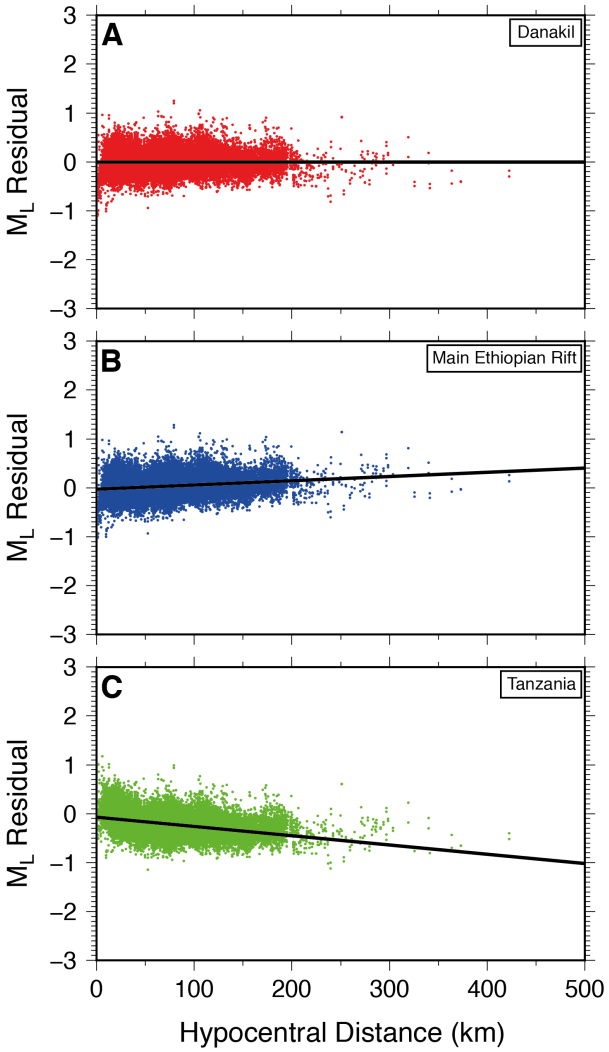

Figure 5: Magnitude residuals calculated for all events using three different scales; the newly derived magnitude scale for (A) Danakil, (B) the Main Ethiopian rift magnitude scale (*Keir et al.*, 2006) and (C) the Tanzania magnitude scale (*Langston et al.*, 1998). The Danakil magnitude scale minimizes residuals at all hypocentral distances whereas the Main Ethiopian rift scale and Tanzania scale overestimate and underestimate magnitudes respectively.

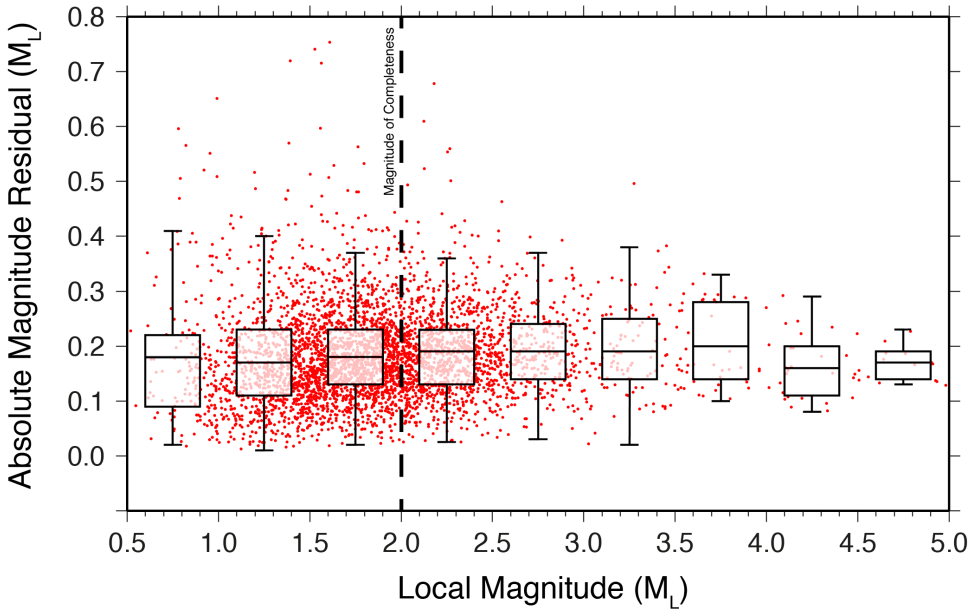

Figure 6: Box plot of magnitude error versus magnitude, binned in 0.5 M_L intervals. Box height represents the interquartile range and whiskers represent extreme values that are within 1.5 interquartile range. Magnitude errors are clearly shown to be stable for the reported magnitude range.

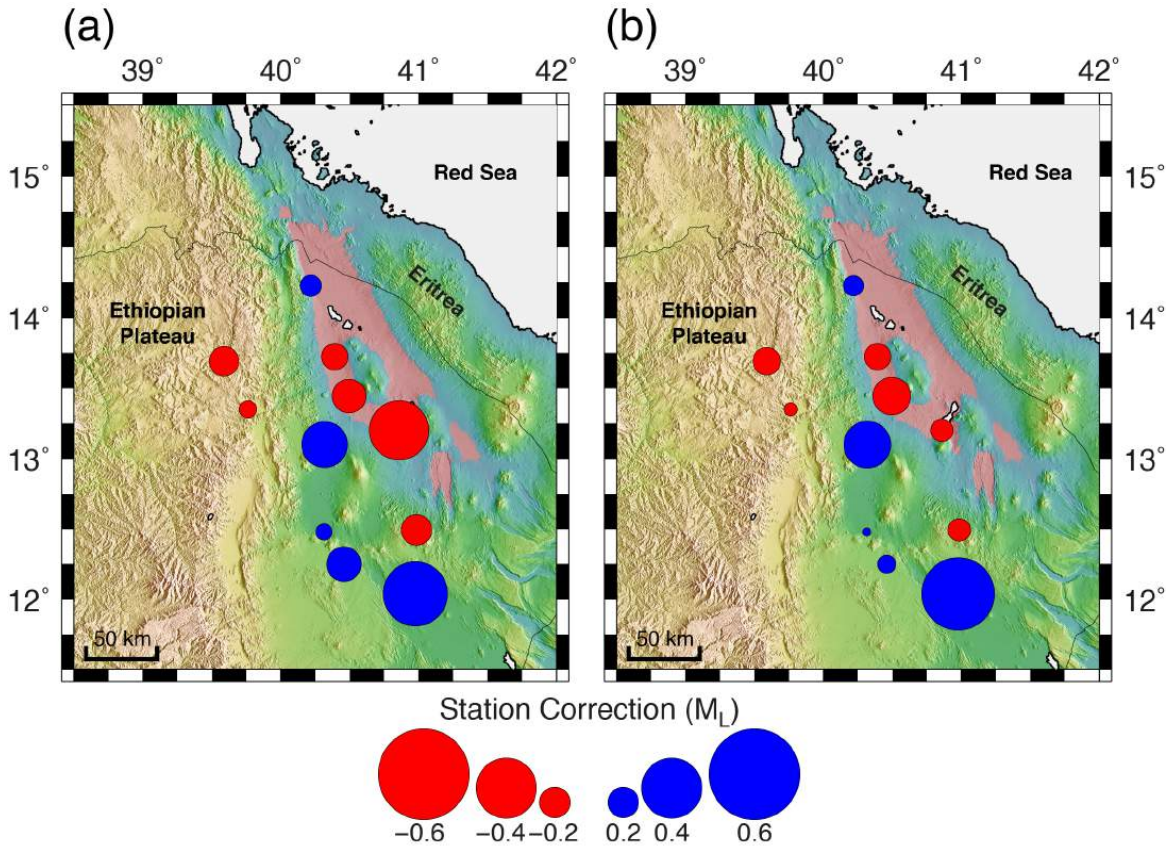

Figure 7: Variation of station corrections across the network. (a) North-south component corrections. (b) East-west component corrections. There is no clear correlation between regional geology and station correction. The corrections are therefore likely controlled by very local geology and site specific variables.

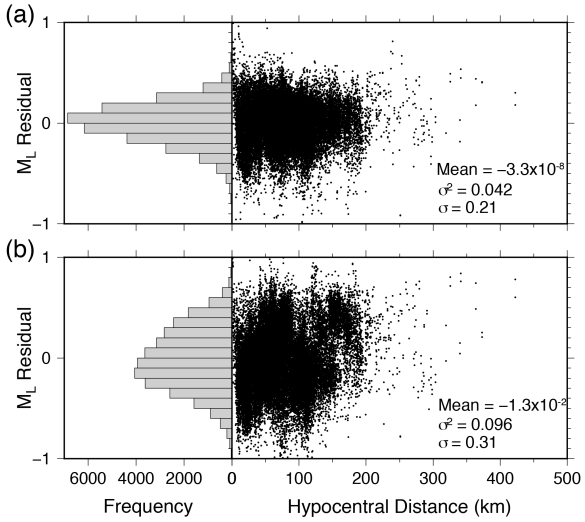

Figure 8: (a) Magnitude residuals calculated with station corrections. (b) Magnitude residuals calculated without station corrections. Magnitude residuals calculated with station corrections sum to nearly zero and the variance (0.042) has been reduced by >64% when compared to the variance without station corrections (0.096).

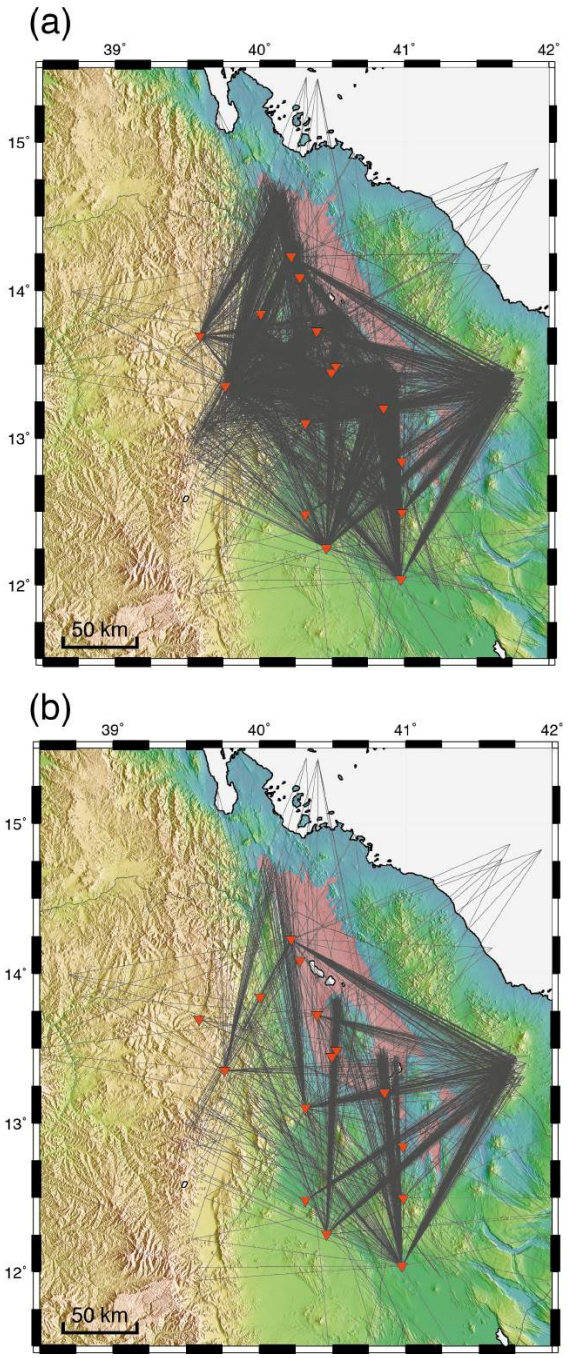

Figure 9: The ray paths for earthquakes with hypocentral distances over (a) 100 km and (b) 150 km. The ray paths predominantly traverse the Danakil depression and Dabbahu segment region.

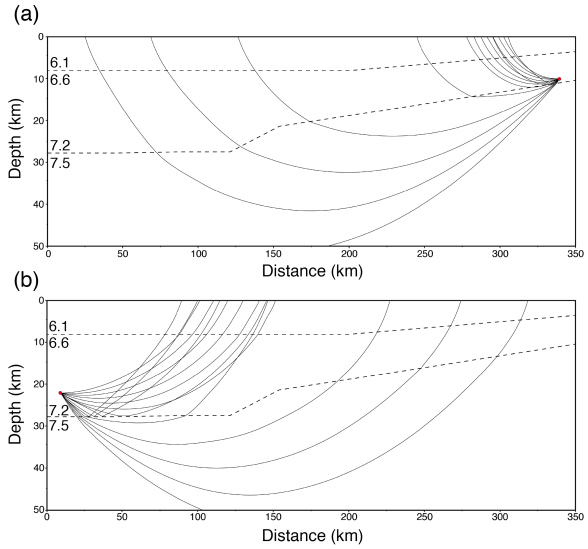

Figure 10: (a) Travel-time curves for an earthquake occurring in the north of the Danakil depression. The S-waves sample the uppermost mantle at hypocentral distances >100 km, reaching depths of up to 40 km. (b) Travel-time curves for an earthquake occurring in the south of the study area. The S-waves sample the uppermost mantle at hypocentral distances >125 km, reaching depths of up to 45 km. Layer P-wave velocities are given in km s^{-1} taken from *Makris and Ginzburg* (1987).

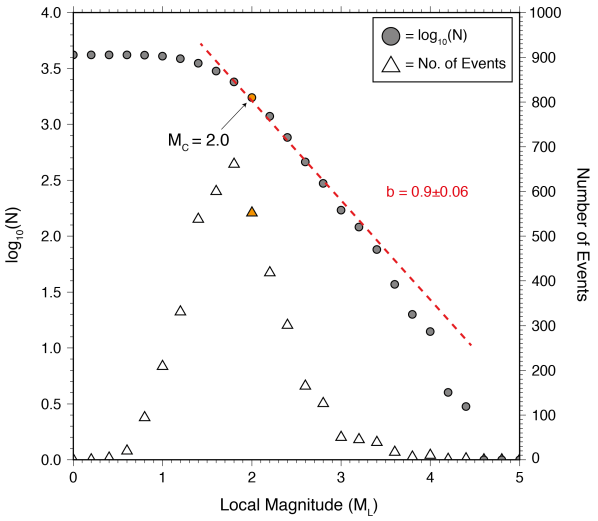

Figure 11: Analysis of earthquake magnitude distribution of earthquakes in the Danakil region, excluding those associated with the eruption of Nabro on 12 June 2011. Left axes - Gutenberg-Richter distribution where log(N) represents the log of the cumulative number of earthquakes of magnitude M_L or greater. Right axes - Number of events represents the frequency of events in each magnitude bin. The magnitude of completeness (2.0 M_L) is calculated using the maximum curvature method (*Wiemer and Wyss*, 2000). We calculate the *b*-value using the maximum likelihood method. The calculated *b*-value suggests that geodetic strain is primarily released through swarms of low magnitude earthquakes, rather than large-scale faulting.